



ELSEVIER

J. Non-Newtonian Fluid Mech. 130 (2005) 129–137

**Journal of
Non-Newtonian
Fluid
Mechanics**

www.elsevier.com/locate/jnnfm

Drag and relaxation in a bentonite clay suspension

 N. Paul Chafe^a, John R. de Bruyn^{a,b,c,*}
^a Department of Physics and Physical Oceanography, Memorial University of Newfoundland, St. John's, Newfoundland, Canada A1B 3X7

^b Laboratoire de Rhéologie, B.P. 53, Domaine Universitaire, Grenoble 38041 Cedex 9, France

^c Department of Physics and Astronomy, University of Western Ontario, London, Ontario, Canada N6A 3K7

Received 8 October 2004; received in revised form 29 July 2005; accepted 8 August 2005

Abstract

We measure the drag force on a sphere moving slowly through a 6% by weight suspension of bentonite clay particles in water. The steady state drag force depends only weakly of the speed of the sphere, indicating that yield stress effects dominate the drag in the range of pulling speeds studied. The drag force increases as a function of time as the suspension gels. The yield stress of the suspension as a function of suspension age is determined from the zero-velocity intercept of our force-pulling speed data. Both the initial transient build-up of the force and its relaxation when the motion stops are described by two exponential time constants, each of which shows an inverse power law dependence on pulling speed. We also determine the yield stress from the force remaining after the relaxation; it is significantly smaller than that determined from the steady-state force data due to the disruption of the structure of the suspension by the motion of the sphere.

© 2005 Elsevier B.V. All rights reserved.

Keywords: Rheological aging; Yield stress; Thixotropic gel; Bingham number

1. Introduction

Bentonite is a smectite clay mineral with many applications that take advantage of its interesting rheological properties in water-based colloidal suspensions [1]. The clay particles are platelets, typically nanometers in thickness and a few microns in diameter. They are positively charged at the edges and negatively charged on their faces. When they are suspended in water at concentrations of a few percent, electrostatic and van der Waals interactions among the particles lead to the formation of a thixotropic gel. This behavior makes bentonite an important component of materials such as drilling muds, paper coatings, and pharmaceutical products. Clay suspensions and related materials are also important in many other contexts, including mud and debris flows [2] and the flow of mine tailings. It is thus of considerable interest to understand the behavior of bentonite suspensions, and from a fundamental point of view to relate their bulk properties to structure and dynamics on the scale of the individual particles.

Bentonite suspensions are pseudoplastic, that is, when sufficiently concentrated they have a yield stress σ_y that results from

the colloidal interactions among the particles. Below the yield stress a suspension behaves as a soft elastic solid, while above σ_y it flows with a shear-thinning behavior. The simplest model for this behavior is the Bingham model [3],

$$\sigma = \sigma_y + K\dot{\gamma}. \quad (1)$$

Here σ is the shear stress, $\dot{\gamma}$ the shear rate, and K the consistency or Bingham viscosity. The Bingham number $Bi = \sigma_y d / K v$, where d is the diameter of the sphere, gives the relative importance of the two terms in Eq. 1. Since the material does not flow if the local stress is less than σ_y , a moving object will be surrounded by a fluidized region in which $\sigma > \sigma_y$, while outside this region $\sigma < \sigma_y$ and the material remains unsheared and solid-like [4].

The motion of a sphere through a yield stress fluid has been studied both experimentally and theoretically by several groups [4–18]. The slow motion of a sphere through a Bingham fluid was studied numerically by Beris et al., who determined the size and shape of the sheared region around the sphere [4]. Further numerical studies taking into account factors such as finite container size and wall slip have been reported in Refs. [5–7].

Early experimental studies of drag in yield-stress fluids include Refs. [8,9]. Atapattu et al. studied the creeping motion of a sphere through Carbopol, a polymer dispersion with a yield stress [10,11]. They studied the effect of nearby walls on the ter-

* Corresponding author.

E-mail address: debruyn@uwo.ca (J.R. de Bruyn).

minimal velocity of a falling sphere [10] and used particle imaging to study the size and shape of the sheared region and the dependence of the drag coefficient on velocity and fluid parameters [11]. Briscoe et al. studied the drag coefficient of spheres falling at their terminal velocity through bentonite clay dispersions [13], and found good agreement with the numerical results of Beris et al. [4]. Jossic and Magnin studied the drag force on objects moving slowly through carboxypol solutions, with particular emphasis on the force required to overcome the yield stress at zero velocity. They also considered the effects of surface roughness and wall slip [14]. Ferroir et al. focussed specifically on the effects of thixotropy on the motion of a sphere through suspensions of laponite [18], and developed a theoretical model for these effects.

The study of bentonite suspensions is complicated by their thixotropy, which involves a time-dependence – or more correctly a dependence on the shear history of the material – of the rheological properties. This behavior is not encompassed by the simple Bingham relation given in Eq. (1), and various attempts have been made to model thixotropy [18–20]. In addition, the properties of our bentonite suspensions change over long times as the material ages, presumably due to slow chemical reactions or dissolution of the clay [21]. Measurements of the rheological properties of bentonite have been reported in a number of publications [19,22–28]; Ref. [1] is a review. Alderman et al. studied the yield stress of bentonite as a function of concentration and noted that σ_y increased with suspension age [23]. Coussot et al. studied the rheology of a bentonite suspension and analyzed their results in the context of a theoretical model for yield stress behavior [19]. Laponite, a synthetic clay which, like bentonite, forms a thixotropic gel when suspended in water, has been studied using a variety of scattering and rheometric techniques [29–36], as have suspensions of other clays with similar properties [2,37].

In this paper, we report on experiments on the drag force on a sphere moving slowly through a 6% by mass bentonite suspension. From the transient changes in force that occur when the motion of the sphere starts and stops, we get information about the processes involved in the break-up and reformation of local structure in the material. The steady-state drag force provides an estimate of the yield stress and Bingham viscosity. Since our measurements are done at very low velocities, yield-stress effects are much larger than viscous contributions to the drag. We also study the changes in behavior over time as the suspension gels.

2. Experiment

We measured the force on a steel sphere while and after it moved at constant speed through a suspension of bentonite clay in water. The experimental apparatus is similar to that described in Ref. [38]. A 0.0254-m steel sphere was attached to a calibrated load cell by a length of monofilament nylon thread [39]. The load cell had a maximum capacity of 2.45 N and a response time that was faster than the interval between recorded data points. It was mounted on a linear actuator which was driven by a computer-controlled stepper motor and the output from the load cell was

recorded by a computer as the sphere was raised and lowered through a column of the sample mixture.

The clay mixture was contained in a PVC cylinder 0.152 m in diameter and 0.605 m tall, closed at the bottom but open at the top. The cylinder was used without any surface treatment, but is large enough that wall effects are not expected to be important [4,10,11]; this issue is discussed further below. The sphere was sequentially raised and lowered through the mixture at a given velocity v , with v varied between 7.6×10^{-4} m/s and 1.02×10^{-2} m/s. A typical run involved 15 cycles of raising and lowering. The length of time the sphere was in motion was varied with the velocity to keep the distance travelled in the range of 0.07–0.1 m. Between periods of raising and lowering the sphere was held at rest for 30 s. When the sphere was in motion the load cell voltage was recorded approximately three times per second. Once the motion was stopped it was recorded every 1.5 s.

The suspension used in the experiments consisted of 6% by weight (2.4% by volume) laboratory grade bentonite (Fisher Scientific B235-500) in deionized water. The maximum particle diameter was approximately $4 \mu\text{m}$ as determined by the sedimentation method [28]. The clay was slowly added to deionized water and mixed for 45 min with an Arrow 1750 mixer. After the initial mixing, the suspension thickened significantly over a time scale of order 20 min as a gel formed. Over the longer term (that is, over several months), the properties of the suspension continued to change slowly, as discussed in the Appendix A. The results presented here were obtained with a suspension that had been prepared 9 months prior to the experiments, then kept in a sealed container. Before each trial, the suspension was remixed for 20 min with the same mixer in an effort to ensure consistent initial conditions. The sphere was positioned on the axis of the cylinder, roughly 0.1 m (four sphere diameters) from the bottom. The bentonite suspension was poured into the cylinder to a depth sufficient to eliminate any surface effects at the high point of the sphere's motion, and the run commenced essentially immediately.

3. Results

Fig. 1 shows the measured force on the sphere as a function of time for one complete cycle of a typical run. Initially the sphere is at rest. When it starts moving upwards the force increases due to the drag on the sphere, but it takes a few seconds for the drag force to reach a steady state value, F_s . When the sphere stops moving, the force on the sphere decays, again over a few seconds, but to a value higher than its initial value. In the second half of the cycle the sphere is lowered and the force decreases, since the direction of the drag force is now upwards, but otherwise the behavior is the same as in the first half of the cycle. In what follows we will not differentiate between data from the raising and lowering parts of the cycle. After lowering, the material is again allowed to relax for 30 s before the cycle is repeated.

Fig. 2 shows the force as a function of time for a full 15-cycle run. The magnitude of the steady state drag force F_s increases over the course of a run as the material properties change. From fits to the individual raising and lowering segments, as described

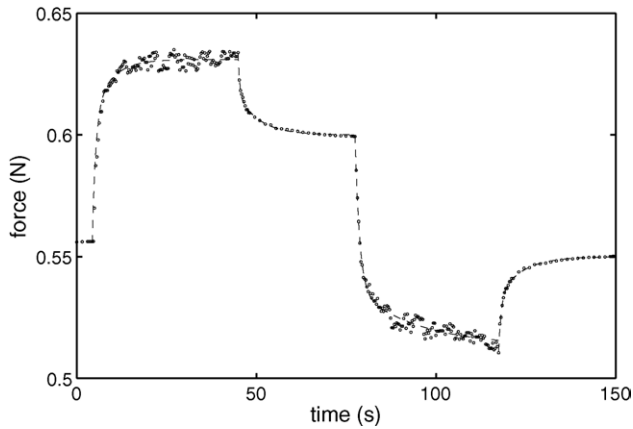


Fig. 1. Force vs. time data measured over one cycle of a typical run as the sphere is raised at speed v , held at rest, lowered at speed v , and then held at rest again. Here $v = 1.78 \times 10^{-3}$ m/s. The dashed lines through the data points are fits of each segment to Eq. (6) (for raising and lowering segments) and Eq. (7) (for relaxation segments). In each case two exponential time constants are required to fit the data.

below, we obtain values for $F_s(T)$, where T is the age of the material measured from the start of the experiment, taken as the midpoint time of each segment. $F_s(T)$ can be described by simple exponential approach to a constant value with a time constant τ_s ,

$$F_s(T) = F_A(1 - e^{-T/\tau_s}) + F_B. \quad (2)$$

A fit to this function is shown by the dashed envelope function in Fig. 2. τ_s is a measure of the time scale for changes in the material properties as it forms a gel. It shows no systematic dependence on pulling speed v , and has a mean value of 540 ± 150 s.

$F_s(0)$ and $F_s(\infty)$, the steady state drag force at zero and infinite time from the start of the run, were found as a function of pulling speed from fits to Eqs. (2) and (6) below. ($F_s(0) = F_B$ in Eq. (2) and $F_s(\infty) = F_A + F_B$). These two quantities are plotted as a function of v in Fig. 3. The measurements at different pulling speeds were performed in random order over a 2-day period. We observed a noticeable dependence of the drag force on

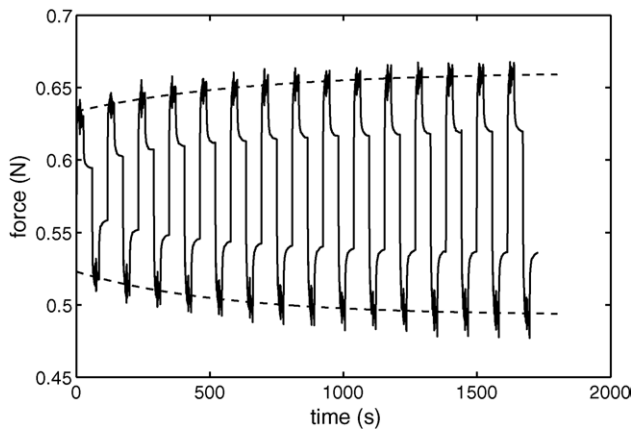


Fig. 2. Force vs. time T for 15 cycles of the experiment. The steady state drag force increases with each cycle as the material's properties change. The dashed line is a fit of the steady state drag force F_s to Eq. (2). Here $v = 3.81 \times 10^{-3}$ m/s.

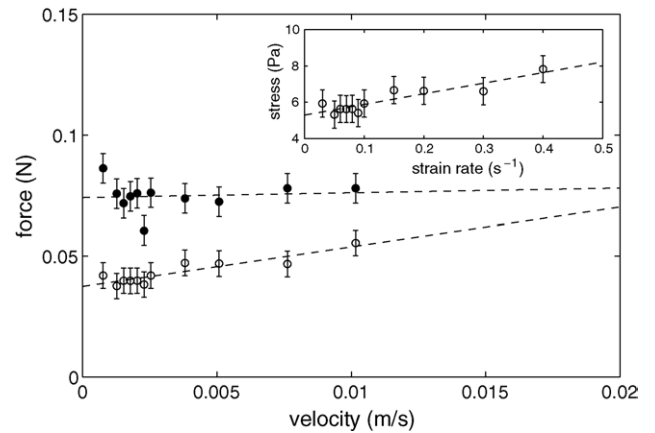


Fig. 3. The steady-state force as a function of pulling speed v , corrected for the aging of the suspension as described in the text. Open circles are for the suspension at $T = 0$ (i.e., immediately after remixing); solid circles are determined from fits to Eq. (2) evaluated at infinite time. The error bars are standard deviations based on averaging results derived from the up- and down-moving segments at each speed. The corresponding Bingham numbers for the $T = 0$ data range from 2.2 at the highest value of v to 30 at the lowest, while for $T \rightarrow \infty$, Bi ranges from 93 to 1240. The dashed lines are linear fits to the data discussed in the text. The inset shows the estimated flow curve at $T = 0$, along with a fit to a Bingham model; the fit gives a yield stress $\sigma_y = 5.3 \pm 0.4$ Pa and a Bingham viscosity $K = (5.9 \pm 2.2) \times 10^{-2}$ Pa s.

the order of measurement; that is, the drag force tended on average to increase from one run to the next, despite the fact that the suspension was remixed before each run, and the variations due to sample aging were at least as large as those due to variations in v . This long term aging is discussed further in the Appendix. In an effort to correct for this, the force data were adjusted to a common reference time by subtracting a term linear in time determined from a fit to the data. The results are presented in Fig. 3. The magnitude of the steady state drag force at $T = 0$ increases slightly with v over the range studied here. Within the accuracy of our measurements the variation is linear, and a fit gives $F_s(0) = (3.8 \pm 0.3) \times 10^{-2} + (1.6 \pm 0.6)v$, with F in N and v in m/s. At infinite age the drag force is larger, but is constant as a function of v within the experimental uncertainty; a fit gives $F_s(\infty) = (7.4 \pm 0.7) \times 10^{-2} + (0.2 \pm 1.5)v$ N. These results indicate that the force on the sphere is almost entirely due to the yield stress, and the viscous contributions are at most 30% in this range of v .

We can estimate the yield stress of this suspension from the zero-velocity intercepts of the plots in Fig. 3. Beris et al. showed numerically that, for a sphere at rest in a Bingham fluid, the force F_y required to overcome the yield stress was given by [4]:

$$F_y = 14\pi r^2 \sigma_y. \quad (3)$$

Applying this result to our data gives a yield stress of 5.3 ± 0.4 Pa at $T = 0$ and 10.4 ± 0.9 Pa as $T \rightarrow \infty$.

Since in our work the viscous contributions to the drag force are small, the Bingham number Bi is expected to be large. As a result, the same conversion from force to stress should be reasonably accurate for the moving sphere as well. We estimate the shear rate to be $\dot{\gamma} = v/d$, where the sphere diameter

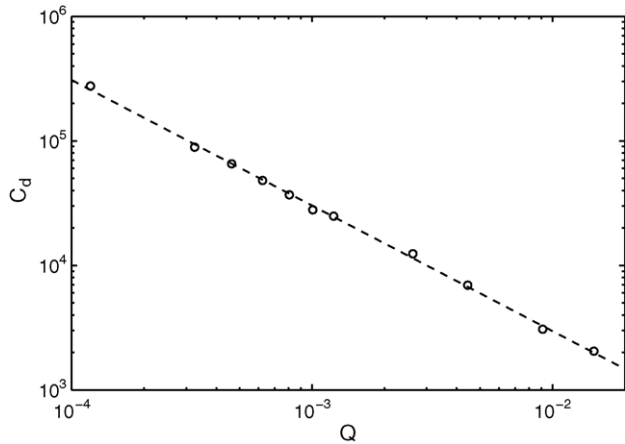


Fig. 4. The drag coefficient corresponding to the steady-state drag force at zero time, $F_s(0)$, plotted as a function of the dimensionless parameter Q defined in the text. The dashed line is a power law fit to the data with an exponent of -1.01 ± 0.03 .

d is an estimate of the size of the sheared region around the sphere [4,11,38], and construct an approximate flow curve for our suspension. This is shown for $T = 0$ in the inset to Fig. 3, and is described within the accuracy of the measurements by a Bingham model with $\sigma_y = 5.3 \pm 0.4$ Pa as above and $K = (5.9 \pm 2.2) \times 10^{-2}$ Pa s. Similarly, for $T \rightarrow \infty$ we find $\sigma_y = 10.4 \pm 0.9$ Pa and $K = (3 \pm 21) \times 10^{-3}$ Pa s. Using these values of σ_y and K , we can calculate the Bingham numbers for our experiments. The results are in the range $2.2 < Bi < 30$ at $T = 0$ and $93 < Bi < 1240$ as $T \rightarrow \infty$, confirming that $Bi \gg 1$ for most of the range covered by our experiments.

Our force data can be non-dimensionalized by defining a drag coefficient C_D in the usual way:

$$C_D = \frac{F}{(1/2)\pi\rho v^2 r^2}. \quad (4)$$

Since F is only weakly dependent on v , C_D is approximately proportional to Bi^2 . A dimensionless quantity that attempts to account for both the yield-stress and viscous contributions to the drag has been used in Refs. [9] and [11]. It is defined by

$$Q = \frac{Re}{1 + kBi} = \frac{\rho v^2}{Kv/D + k\sigma_y}, \quad (5)$$

where Re is a modified Reynolds number and k is a constant given in Ref. [9] as $7\pi/24$. We plot C_D as a function of Q for the zero-age data in Fig. 4. C_D is proportional to Q^{-1} over the range of our data, which again reflects the fact that the drag in this case is dominated by the yield stress while the viscous contribution is small. These results are in excellent agreement with those of Refs. [9,11].

The transient approach of the force to its steady state value when the sphere starts moving is well described by the sum of two exponential terms,

$$F(t) = F_1(1 - e^{-t/\tau_{m1}}) + F_2(1 - e^{-t/\tau_{m2}}) + F_0, \quad (6)$$

where t is the time (measured from the start of the sphere's motion for each segment), τ_{m1} and τ_{m2} are time constants, F_1

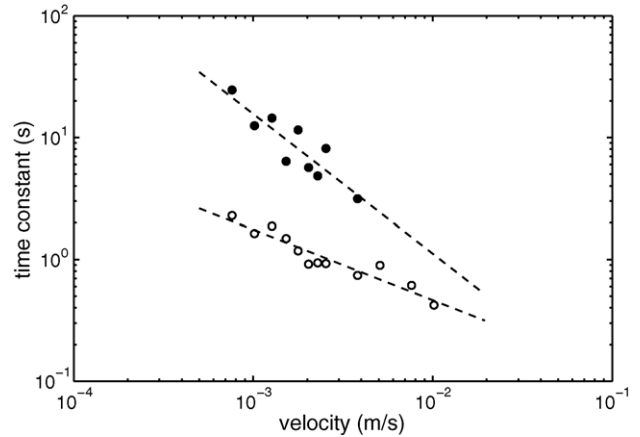


Fig. 5. The two time constants τ_{m1} and τ_{m2} associated with the build-up of the drag force when the sphere starts to move, plotted as a function of v . Open circles are τ_{m1} and solid circles are τ_{m2} . The dashed lines are power law fits which give power law exponents of -0.58 ± 0.06 and -1.15 ± 0.22 , respectively. Note that, within our uncertainties, there is no term involving τ_{m2} at the higher values of v .

and F_2 are the amplitudes of the exponential terms and F_0 is the force measured when the sphere is at rest at time zero. The steady-state drag force acting on the sphere is $F_s = F_1 + F_2$. Fits to this function for both the raising and lowering segments of the data are shown as dashed lines in Fig. 1. Except as described below, a function with only one exponential term is not adequate to describe the transient, and the presence of two time constants indicates that there are two distinct processes involved in the build-up of the force.

The relaxation of the drag force when the motion of the sphere stops is also well described by a sum of two exponential terms. We fit the relaxation data to the form

$$F(t) = R_1 e^{-t/\tau_{r1}} + R_2 e^{-t/\tau_{r2}} + R_0, \quad (7)$$

where τ_{r1} and τ_{r2} are the time constants for the relaxation, R_1 and R_2 are the corresponding amplitudes, and R_0 is force as t goes to infinity. As above, the presence of two time constants indicates that two processes contribute to the relaxation. Fits of Eq. (7) to the decaying segments of the data are also shown in Fig. 1.

Within the experimental scatter, the two time constants τ_{m1} and τ_{m2} which characterize the transient build-up of the drag force remain constant over the course of a run, indicating that they are not affected by the gelation or aging of the material. At high v , only the shorter time constant τ_{m1} is required to describe the transient; the term with the longer time constant goes to zero as described below. In addition, the force transient for the first raising segment in each run has only the shorter time constant, indicating that the character of the fluid when freshly poured is qualitatively different from that even a minute later. τ_{m1} and τ_{m2} are plotted as a function of v in Fig. 5. Each point in this figure is an average over the 30 upward and downward segments of a run. Both τ_{m1} and τ_{m2} show an inverse power law dependence on pulling speed (or equivalently, on shear rate) over the range studied.

τ_{m2} , the longer time constant, is approximately inversely proportional to v ; a fit gives $\tau_{m2} = (5.5 \pm 2.0) \times 10^{-3} v^{-1.15 \pm 0.22}$ s (with v , here and elsewhere, in m/s). We identify this as the time scale for the establishment of the sheared region around the sphere when it starts to move [38]. The flow induced by the moving sphere disrupts the local structure of the suspension to some distance δ , and the time scale for this disruption to develop is just δ/v , the time it takes for the sphere to move δ . Our results indicate that $\delta \approx 0.011$ m, slightly smaller than the radius of the sphere. At the start of the first segment of each run, the suspension is already fully fluidized from the mixing and from being poured into the experimental container. There is thus no need for the sphere to establish a sheared region around itself in this case — the material is already sheared. This explains the absence of the τ_{m2} term for this first segment. At later times, the suspension has begun to gel and this term appears.

The shorter time constant τ_{m1} has a weaker dependence on pulling speed: a fit gives $\tau_{m1} = (3.2 \pm 0.3) \times 10^{-2} v^{-0.58 \pm 0.06}$ s. The strength of the material depends on interactions among the suspended clay platelets, which in turn depend on local variations of the particle positions and orientations. One would expect these to adjust diffusively to changes in the local environment, and we suggest that τ_{m1} is the time scale for the response to changes in the structure of the material in the region immediately around the sphere.

For the first raising segment of each run, $F_2 = 0$ since, as noted above, only the F_1 term is needed to describe the force transient. Thereafter, the relative size of the F_1 term decreases slightly with time while that of the F_2 term (due to shear) increases, indicating that more work is required to fluidize the material as its gelation progresses. Fig. 6 shows the relative sizes of F_1 and F_2 as a function of pulling speed v at a particular time. The relative magnitude of the shear term decreases as v increases, while that of the F_1 term increases. For $v \gtrsim 5 \times 10^{-3}$ m/s, our fitting program is unable to discern the F_2 term and the transient is well described by a single exponential term with the time constant τ_{m1} . The disappearance of the term due to shear is likely because the structure of the region around the sphere is sufficiently disrupted at high v that it is not necessary to re-establish the sheared region in each cycle of the experiment.

The time constants τ_{r1} and τ_{r2} characterizing the relaxation of the drag force are plotted as a function of v in Fig. 7. These data were also averaged over all cycles of each run. Despite that fact that the sphere is now motionless, both depend on the previous velocity, and by inference are related to processes taking place within the sheared region created by the previous motion of the sphere. As in the case of motion, the shorter time constant τ_{r1} behaves approximately as $v^{-1/2}$: $\tau_{r1} = (2.9 \pm 0.2) \times 10^{-2} v^{-0.50 \pm 0.03}$ s. As before we identify this as the time constant for relaxation of stress due to diffusive changes in the structure of the material in the sheared region around the sphere. The shorter magnitude in this instance is likely a result of the fact that the motion of the sphere through the suspension has disrupted the structure of the material, reducing the viscosity and so the response time below that at the onset of shear.

τ_{r2} , the larger relaxation time constant, also decreases with increasing velocity, but with a significantly weaker dependence

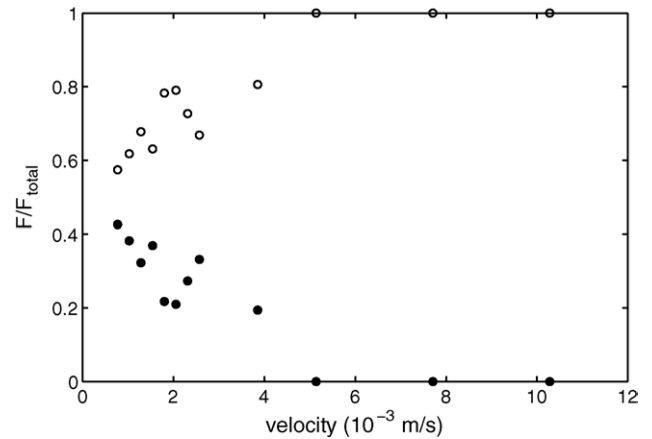


Fig. 6. The relative contribution of each of the two components of the transient build-up of the drag force as a function of v at time $T \approx 400$ s. The open symbols represent $F_1/(F_1 + F_2)$ and the solid symbols $F_2/(F_1 + F_2)$. For $v \gtrsim 5 \times 10^{-3}$ m/s, $F_2 = 0$ within our uncertainties and the transient is well described by a single time constant.

on v . A fit gives $\tau_{r2} = (0.94 \pm 0.02) v^{-0.30 \pm 0.02}$ s. The associated stress relaxation process is likely related to some sort of healing of the fluidized region, although its exact nature is unclear.

Fig. 8 shows the relative contributions of the R_1 and R_2 terms to the relaxation of the drag force as a function of v at a particular time. Although the variation with (previous) pulling speed is weaker than was the case for the build-up of the force, the relative importance of the R_1 term increases slightly and that of the R_2 term decreases as v increases.

The stress remaining on the sphere after the relaxation process has finished should be simply equal to the yield stress itself, since it is the stress measured at zero shear rate [40]. The force remaining after relaxation, R_0 , was obtained from fits to Eq. (7) and as before converted to a yield stress using Eq. (3). As with other quantities, σ_y determined in this way is a function of the time T from the beginning of the experiment, and the variation with T is well described by an exponential function similar to Eq.

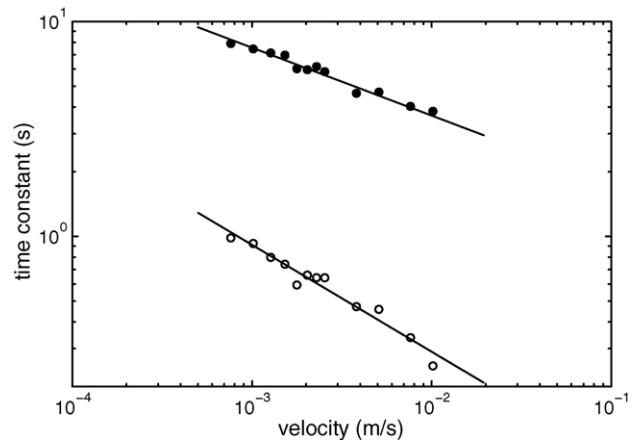


Fig. 7. τ_{r1} and τ_{r2} , the two time constants associated with the relaxation of the force after the sphere is stopped, plotted as a function of v . Open circles are τ_{r1} and solid circles are τ_{r2} . The lines are power-law fits to the data and give exponents of -0.50 ± 0.03 and -0.30 ± 0.02 , respectively.

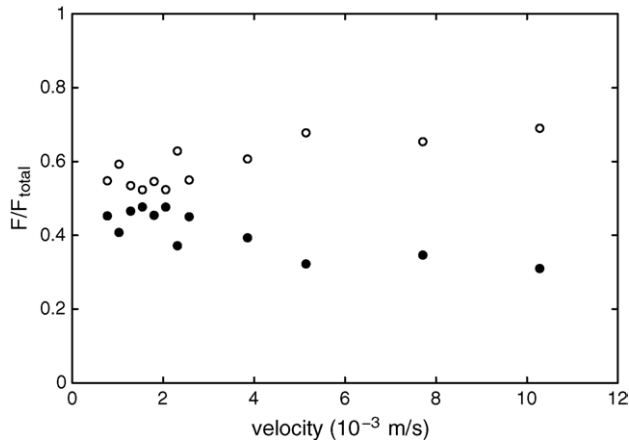


Fig. 8. The relative contribution of each of the two components of the force during relaxation plotted as a function of v at time $T \approx 600$ s. The open symbols represent $R_1/(R_1 + R_2)$ and the solid symbols $R_2/(R_1 + R_2)$.

(2) with a time constant of 500 ± 130 s. Averaging over all runs we find $\sigma_y(0) = 1.60 \pm 0.35$ Pa and $\sigma_y(\infty) = 5.20 \pm 0.65$ Pa. The values of σ_y obtained in this way are significantly lower than those obtained at the same values of T from the $v = 0$ intercept of the drag force, as described above. We interpret this as a manifestation of the thixotropic nature of the suspension: the motion of the sphere through the suspension disrupts the structure of the gel and consequently reduces the yield stress. As a result, the yield stress measured immediately after the suspension has been sheared is lower than that measured after the suspension has had some time to restructure. Alternatively, it could be a result of the presence of a minimum in the flow curve for bentonite suspensions, as observed by Coussot et al. [19].

4. Discussion

We first discuss some effects that might influence our measurements of the drag force. Wall effects are expected to contribute to the drag when the sheared region around the moving sphere extends to the container wall [15]. In the present case the container radius is six times the radius of the sphere and Bi is, for the most part, large. Experiments [10,11] and simulations [4,6] suggest that the extent of the sheared region is on the order of four times the sphere radius and decreases with increasing Bi . This suggests that wall effects should be relatively unimportant in the present work. Numerical work by Blackery and Mitsoulis [6] for a container radius four times the sphere radius found that the sheared region extended to the container walls for $Bi \lesssim 2.3$, which also indicates that for our geometry and range of Bi , wall effects should be small. The experiments of Ref. [10] do not extend into the parameter range studied here, but extrapolation of their results give a ratio of free-fall terminal velocities with and without walls for our geometry of approximately 0.85. Our own measurements suggest that the effect is significantly smaller than this. Buoyant forces in yield-stress fluids have not been considered in much detail but if we assume that the pressure within our suspension is simply hydrostatic, then the buoyant force on the sphere will be the same for both upward

and downward portions of the experiment and will not affect our measurements.

The existence of a yield stress results from an internal structure within the fluid — in the present case, due to interactions among the suspended clay particles. Shear disrupts this structure and fluidizes the material, reducing its viscosity. On the cessation of shear (and neglecting aging effects), the internal structure reforms and the fluid properties return to their original values. This restructuring takes time; this is the origin of the thixotropy of the suspension. The reformation of structure following shear is distinct from, but presumably closely related to, the gelation of the material over time, which takes place in the unsheared material.

The bentonite suspension was remixed before each run, completely disrupting any pre-existing structure in the material. As the experiment progresses, the properties of the suspension change as structure reforms and the material gels. Both the steady-state drag force and the yield stress determined after relaxation of the drag force show an exponential approach to a constant value, with a time constant of 540 ± 150 s in the first case and 500 ± 130 s in the second case. These values are the same within our uncertainties. No systematic variation of this gelation time with experimental parameters or with the age of the sample was observed, although the uncertainties are fairly large due to scatter from run to run. The drag force and yield stress increase with time, despite the fact that the motion of the sphere periodically disrupts the structure in the region around it. This suggests that the formation of structure in the sheared region around the sphere is influenced by the state of the suspension in the surrounding, undisturbed material. In scattering experiments on laponite suspensions, Kroon et al. showed that gelation involves the partial development and then decay of orientational order among the clay platelets [33,34]. They found the gelation time to decrease exponentially with the mass fraction of the clay. Extrapolating their data to a mass fraction of 6% gives a gelation time of order 100 s, a factor of five lower than observed here.

We obtained estimates of the yield stress of our suspension in two ways: first, from the zero-velocity intercept of our force versus velocity data, as in Fig. 3, and second from the force remaining on the sphere after relaxation. As noted above, the values obtained after relaxation are lower than those from the steady-state drag force. The motion of the sphere through the material disrupts the existing structure and so reduces the yield stress, and as a result the yield stress measured at the end of a cycle when the motion stops is less than at the beginning of a cycle. The implication of this is that, although the overall gelation time is of order 500 s, the local structure in the sheared region around the sphere heals significantly over the 30 s that the sphere is at rest between segments.

A number of measurements of the yield stress of bentonite suspensions have been reported [19,22–28]. Although the value of the yield stress will depend on the details of the material used and on how the measurements were done, it is nonetheless useful to compare our results to the previous work. Our result from the zero-velocity intercept of the force–velocity data is 5.3 ± 0.4 Pa immediately after remixing, and increases as the

suspension gels. This is somewhat higher than the value of 2.8 Pa measured by Alderman et al. for a 5.83% suspension using vane rheometry or the value of 2.2 Pa for a 6% suspension obtained from analysis of the flow of a sheet of the suspension down an inclined plane [28]. On the other hand, the value of σ_y obtained after the cessation of motion is 1.60 ± 0.35 Pa at age zero, which is closer to the previous results and is probably a better estimate of σ_y for the freshly sheared suspension. Our observation that σ_y increases with age is consistent with previous work [23] and with the simple observation that the suspension gels over time. It is evident, however, that the determination of σ_y here depends not only on the time after mixing but also on the shear history and the state of the entire sample. While the same is true of simple shear flows in thixotropic fluids, we would expect our values of σ_y to be less accurate than those obtained by careful rheometric measurements. In addition, there are two potentially significant sources of systematic uncertainty in our determination of σ_y . First, we have used Eq. (3) to convert our force measurements into stresses. This approach should be valid for our measurements, since Bi is large when the sphere is moving and infinite when it is at rest, but there remains the assumption that the numerical factor in Eq. (3), determined from numerical simulations [4], is correct for our system, and indeed the assumption that the Bingham model describes this material adequately. Second, wall slip may be present at the surface of the sphere and affect our measurements of the drag force when the sphere is moving (but not when it is at rest). In similar experiments using carbopol, a difference of about 40% was observed between measurements using rough and smooth spheres [14]. The presence of slip would lead to an underestimation of the yield stress from the force–velocity data.

Our measurements show a linear increase in drag force as a function of v for the freshly mixed suspension. At later times as the suspension gels, the drag force becomes independent of v and so is due entirely to the yield stress. Equivalently, the stress is independent of shear rate over the range covered. Reliable measurements of the Bingham viscosity K in the literature are few and are based on measurements done over a much wider range of shear rates, and the uncertainties in our values of K are large, so a meaningful comparison with our results is difficult. Jossic and Magnin observed that the drag force they measured in carbopol was independent of speed for low speeds [14], and a velocity-independent drag force has also been observed in a dry granular medium [41].

When the sphere starts to move in the suspension, one would expect the medium to respond elastically (i.e., linearly) until a yield strain is exceeded and the material fluidizes. In fact, this elastic regime is not particularly evident in our force–time data, probably because we do not have sufficient time resolution at the beginning of each cycle to distinguish it. Both the transient development of the stress at the onset of motion and its relaxation when the motion is stopped are nonexponential in time and can be fitted by functions with two exponential terms. This indicates that two distinct processes are involved in the build up and relaxation of stress in this suspension. All four time constants — two for build-up and two for relaxation — show an inverse power law dependence on v (or, equivalently, on shear rate).

t_{m2} is roughly inversely proportional to shear rate. In similar experiments on aqueous foam [38], the build-up of the drag force was characterized by a single time constant which was also inversely proportional to $\dot{\gamma}$. As in that work, we associate this time scale with the time required for the sheared region around the sphere to develop as the sphere moves. The shorter of the two time constants for motion and relaxation, t_{m1} and t_{r1} , respectively, are both approximately proportional to $1/v^{1/2}$ and have about the same magnitude, so it is reasonable to infer that they are due to the same process, and that this process is similar whether the sphere is moving or not. The gelation process in clay suspensions involves positional and orientational diffusion of the clay platelets [33], and we suggest that these time scales are associated with a diffusive response to the local disruption — in the case of the build up of the drag force — or the reforming — in the case of relaxation — of orientational or positional organization in the material. Since as shown in Fig. 3 the stress is roughly constant as a function of shear rate, the viscosity of the suspension is inversely proportional to v , and so the diffusion constant $D \propto v$. The time for diffusion over a distance λ would be λ^2/D and thus inversely proportional to v . However, one could imagine that the distance scale λ could increase weakly with v , since a faster-moving object would cause a more serious disruption of the local structure. In this case, the v dependence of the diffusive time scale would be weaker than linear, as observed. The longer time scale for the relaxation of the stress, t_{r2} , is proportional to $v^{-0.3}$. The same v dependence was observed in one component of the relaxation of the drag force in similar experiments on foam [38], in which case the relaxation was related to local restructuring of the foam following the cessation of shear. Here again this process must be related to the redevelopment of structure and relaxation of stress in the sheared region, although further study is required to determine its exact nature. These time constants are all significantly shorter than the relaxation and restructuring times, as defined in the theoretical model of Coussot et al. found for a bentonite suspension in Ref. [19]. We note also that the creep compliance of bentonite suspensions has also been found to involve two time constants [25].

Rheological aging in so-called soft glassy materials has recently been studied both theoretically [42,43] and experimentally [44–47]. In this phenomenon, the structure and properties of the material change slowly with time but, since the relaxation time itself increases with sample age, the system never reaches a steady state. Our experiment is not particularly well suited to the study of rheological aging and we note that our measured drag force does appear to approach a steady state value at long times. Harden et al. have studied aging in suspensions of laponite clay using a combination of scattering techniques and observed a complex aging behavior [44–46]. At concentrations high enough that the laponite formed a gel, they observed a fast relaxation of the scattering correlation function which they attribute to diffusion, and a much slower process which they attribute to processes that relax stress locally [46]. These relaxation processes may be related to those seen here.

It is interesting to compare the results presented here to those obtained in similar experiments on an aqueous foam [38]. In that

case, the transient build-up of the drag force was well described by a single exponential term, with a time constant inversely proportional to shear rate. This time constant is apparently analogous to τ_{m2} in the present case, but τ_{m1} , which here we attribute to a time scale for adjustments in the position or orientation of the clay platelets, is not present in the foam case. This is reasonable, since there is no analogous process in the foam. Three time constants were required to adequately describe the relaxation of the drag force in foam, compared to two in the present case. The shortest of these was of order one second and decreased weakly with the previous shear rate as $\dot{\gamma}^{-0.3}$. As discussed above, this is the same shear rate dependence as shown by τ_{r2} in the present work and is likely related to a healing of the material structure in the previously sheared region surrounding the sphere. The diffusive time scale is again absent from the relaxation in the foam, with the two longer time scales in that case being roughly independent of shear rate and of order 10 and a few hundred seconds. These times were associated with the time between local bubble rearrangements and coarsening of the bubble size distribution, respectively, both processes that do not occur in the clay suspension.

5. Conclusions

We have studied the drag force on a sphere moving through a 6% by mass bentonite suspension. The build-up and relaxation of the force are nonexponential, indicating that two distinct processes contribute to the disruption and reforming of structure within the sheared region surrounding the sphere. The steady state drag force increases weakly with the speed of the sphere for the freshly remixed, and not at all for a suspension which has had time to gel. This indicates that the drag force in this material is almost entirely due to the yield stress. The yield stress increases with time as the suspension forms a gel, with a gelation time of roughly 520 s.

Acknowledgements

This research was supported by NSERC of Canada and CNRS, France.

Appendix A. Suspension aging

The bentonite suspension studied shows long-term aging effects in addition to the shorter-term time dependence due to gelation described above. This slower aging is likely due to slow chemical changes in the material as a result of its exposure to air [21], and is also distinct from the rheological aging mentioned above [42,43]. The effect of this (chemical) aging is illustrated in Fig. A.1, which shows $F_s(\infty)$, the infinite-time steady-state drag force, as a function of the age of the sample for a pulling speed of $v = 5.08 \times 10^{-3}$ m/s. The data were obtained from two different suspensions that were prepared identically. The point at age zero was obtained immediately after the suspension was prepared. All other data were obtained from a second suspension that had been prepared and then covered for approximately 6 months before any measurements were taken. Fig. A.1 shows

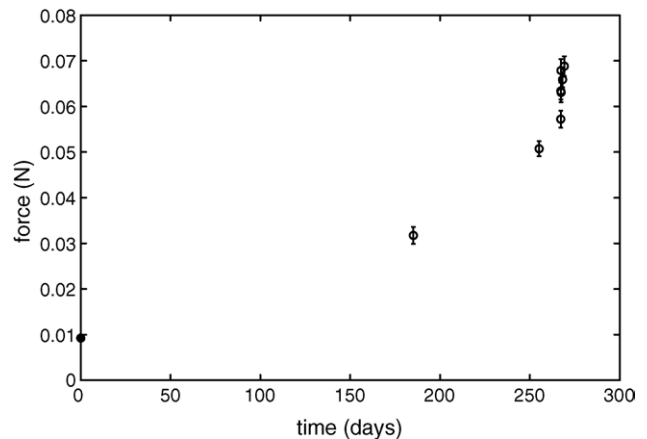


Fig. A.1. The steady state drag force at infinite time $F_s(\infty)$ for $v = 5.1 \times 10^{-3}$ m/s plotted as a function of the age of the suspension, measured from when it was first prepared. The different symbols correspond to two identically prepared suspensions that differed in their date of preparation only. The open circles were obtained from a suspension that had remained covered for approximately 6 months after preparation before being first used, while the solid circle is for a suspension that was used immediately after preparation.

a steady increase in the drag force as the material ages over a period of a few months, followed by a more sudden increase at an age of approximately 265 days. This increase corresponds to a period of more frequent experimentation over a 1-week period. The repeated mixing and pouring of the suspension during this time exposed it to the air much more than when it was sitting in a covered container and accelerated the chemical changes occurring. To minimize the effect of this chemical aging on our results, the data reported in this paper were collected over a 2 day period at an age of 267 days.

References

- [1] P.F. Luckham, S. Rossi, The colloidal and rheological properties of bentonite suspensions, *Adv. Colloid Interf. Sci.* 82 (1999) 43.
- [2] P. Coussot, *Mudflow Rheology and Dynamics*, Balkema, Rotterdam, 1997.
- [3] R.W. Whorlow, *Rheological Techniques*, Ellis Horwood, New York, 1992.
- [4] A.N. Beris, J.A. Tsamopoulos, R.C. Armstrong, R.A. Brown, Creeping motion of a sphere through a Bingham plastic, *J. Fluid Mech.* 158 (1985) 219.
- [5] M. Beaulne, E. Mitsoulis, Creeping motion of a sphere in tubes filled with Herschel-Bulkley fluids, *J. Non-Newtonian Fluid Mech.* 72 (1997) 55.
- [6] J. Blackery, E. Mitsoulis, Creeping motion of a sphere in tubes filled with a Bingham plastic material, *J. Non-Newtonian Fluid Mech.* 70 (1997) 59.
- [7] B. Deglo De Besses, A. Magnin, P. Jay, Sphere drag in a viscoplastic fluid, *AIChE J.* 50 (2004) 2627.
- [8] L. Valentik, R.L. Whitmore, The terminal velocity of spheres in Bingham plastics, *Br. J. Appl. Phys.* 16 (1965) 1197.
- [9] R.W. Ansley, T.N. Smith, Motion of spherical particles in a Bingham plastic, *AIChE J.* 13 (1967) 1193.
- [10] D.D. Atapattu, R.P. Chhabra, P.H.T. Uhlherr, Wall effect for spheres falling at small Reynolds number in a viscoplastic medium, *J. Non-Newtonian Fluid Mech.* 38 (1990) 31.
- [11] D.D. Atapattu, R.P. Chhabra, P.H.T. Uhlherr, Creeping sphere motion in Herschel-Bulkley fluids: flow field and drag, *J. Non-Newtonian Fluid Mech.* 59 (1995) 245.
- [12] M. Hariharaputhiran, R.S. Subramanian, G.A. Campbell, R.P. Chhabra, The settling of spheres in a viscoplastic fluid, *J. Non-Newtonian Fluid Mech.* 79 (1998) 87.

- [13] B.J. Briscoe, M. Glaese, P.F. Luckham, S. Ren, The falling of spheres through Bingham fluids, *Colloid Surf.* 65 (1992) 69.
- [14] L. Jossic, A. Magnin, Drag and stability of objects in a yield stress fluid, *AIChE J.* 47 (2001) 2666.
- [15] For a review, see R.P. Chhabra, *Bubbles, Drops and Particles in Non-Newtonian Fluids*, CRC Press, London, 1993.
- [16] E. Mitsoulis, On creeping drag flow of a viscoplastic fluid past a circular cylinder: wall effects, *Chem. Eng. Sci.* 59 (2004) 789.
- [17] T. Zisis, E. Mitsoulis, Viscoplastic flow around a cylinder kept between parallel plates, *J. Non-Newtonian Fluid Mech.* 105 (2002) 1.
- [18] T. Ferroir, H.T. Huynh, X. Chateau, P. Coussot, Motion of a solid object through a pasty (thixotropic) fluid, *Phys. Fluids* 16 (2004) 594.
- [19] P. Coussot, A.I. Leonov, J.-M. Piau, Rheology of concentrated dispersed systems in a low molecular weight matrix, *J. Non-Newtonian Fluid Mech.* 46 (1993) 179.
- [20] J. Mewis, Thixotropy—A general review, *J. Non-Newtonian Fluid Mech.* 6 (1979) 1.
- [21] D.W. Thompson, J.T. Butterworth, The nature of laponite and its aqueous dispersions, *J. Colloid Interf. Sci.* 151 (1992) 236.
- [22] B.J. Briscoe, P.F. Luckham, S.R. Ren, An assessment of a rolling-ball viscometer for studying non-Newtonian fluids, *Coll. Surf.* 62 (1992) 153.
- [23] N.J. Alderman, G.H. Meeten, J.D. Sherwood, Vane rheometry of bentonite gels, *J. Non-Newtonian Fluid Mech.* 39 (1991) 291.
- [24] H. Heller, R. Keren, Rheology of Na-rich Montmorillonite suspensions affected by electrolyte concentration and shear rate, *Clay Clay Miner.* 49 (2001) 286.
- [25] K. Bekkour, N. Kherfella, Linear viscoelastic behavior of bentonite-water suspensions, *Appl. Rheol.* 12 (2002) 234.
- [26] K. Bekkour, H. Ern, O. Scrivener, Rheological characterization of bentonite suspensions and oil-in-water emulsions loaded with bentonite, *Appl. Rheol.* 11 (2001) 178.
- [27] H. van Damme, C. Laroche, L. Gatineau, Radial fingering in viscoelastic media, an experimental study, *Rev. Phys. Appl.* 22 (1987) 241.
- [28] J.R. de Bruyn, P. Haddas, S. Kim, Fingering instability of a sheet of yield-stress fluid, *Phys. Rev. E* 66 (2002) 031504.
- [29] F. Pignon, J.-M. Piau, A. Magnin, Structure and pertinent length scale of a discotic clay gel, *Phys. Rev. Lett.* 76 (1996) 4857.
- [30] F. Pignon, A. Magnin, J.-M. Piau, Butterfly light scattering pattern and rheology of a sheared thixotropic clay gel, *Phys. Rev. Lett.* 79 (1997) 4689.
- [31] F. Pignon, A. Magnin, J.-M. Piau, Thixotropic behavior of clay dispersions: combinations of scattering and rheometric techniques, *J. Rheol.* 42 (1998) 1349.
- [32] D. Bonn, H. Kellay, H. Tanaka, G.H. Wegdam, J. Meunier, Laponite: what is the difference between a gel and a glass?, *Langmuir* 15 (1999) 7534.
- [33] M. Kroon, W.L. Vos, G.H. Wegdam, Structure and formation of a gel of colloidal disks, *Phys. Rev. E* 57 (1998) 1962.
- [34] M. Kroon, G.H. Wegdam, R. Sprik, Dynamic light scattering studies on the sol-gel transition of a suspension of anisotropic colloidal particles, *Phys. Rev. E* 54 (1996) 6541.
- [35] B. Abou, D. Bonn, J. Meunier, Aging dynamics in a colloidal glass, *Phys. Rev. E* 64 (2001) 021510.
- [36] A. Mourchid, A. Delville, J. Lambard, E. Lécolier, P. Levitz, Phase diagram of colloidal dispersions of anisotropic charged particles: equilibrium properties, structure, and rheology of laponite suspensions, *Langmuir* 11 (1995) 1942.
- [37] P. Coussot, Structural similarity and transition from Newtonian to non-Newtonian behavior for clay-water suspensions, *Phys. Rev. Lett.* 74 (1995) 3971.
- [38] J.R. de Bruyn, Transient and steady-state drag in foam, *Rheol. Acta* 44 (2005) 150.
- [39] Following Ref. [14], we estimate the drag force on the thread itself to be only of order 1% of the total drag.
- [40] A. Magnin, J.M. Piau, Cone and plate rheometry of fluids with a yield stress, *J. Non-Newtonian Fluid Mech.* 36 (1990) 85.
- [41] R. Albert, M.A. Pfeifer, A.-L. Barabási, P. Schiffer, Slow drag in a granular medium, *Phys. Rev. Lett.* 82 (1999) 205.
- [42] P. Sollich, F. Lequeux, P. Hébraud, M.E. Cates, Rheology of soft lassy materials, *Phys. Rev. Lett.* 78 (1997) 2020.
- [43] P. Sollich, Rheological constitutive equation for a model of soft glassy materials, *Phys. Rev. E* 58 (1998) 738.
- [44] A. Knaebel, M. Bellour, J.-P. Munch, V. Viasnoff, F. Lequeux, J.L. Harden, Aging behavior of Laponite clay particle suspensions, *Europhys. Lett.* 52 (2000) 73.
- [45] M. Bellour, A. Knaebel, J.L. Harden, F. Lequeux, J.-P. Munch, Aging processes and scale dependence in soft glassy colloidal suspensions, *Phys. Rev. E* 67 (2003) 031405.
- [46] R. Bandyopadhyay, D. Liang, H. Yardimci, D.A. Sessoms, M.A. Borthwick, S.G.J. Mochrie, J.L. Harden, R.L. Leheny, *Phys. Rev. Lett.* 93 (2004) 228302.
- [47] M. Cloitre, R. Borrega, L. Leibler, Rheological aging and rejuvenation in microgel pastes, *Phys. Rev. Lett.* 85 (2000) 4819.